Relationship between phonons and thermal expansion in $Zn(CN)_2$ and $Ni(CN)_2$ from inelastic neutron scattering and *ab initio* calculations

R. Mittal,[1] M. Zbiri,[2] H. Schober,[2,3] E. Marelli,[4] S. J. Hibble,[4] A. M. Chippindale,[4] and S. L. Chaplot[1]

[1]*Solid State Physics Division, Bhabha Atomic Research Centre, Trombay, Mumbai 400 085, India*

[2]*Institut Laue-Langevin, BP 156, F-38042 Grenoble Cedex 9, France*

[3]*Université Joseph Fourier, Unité de Formation et de Recherche (UFR) de Physique, F-38041 Grenoble Cedex 9, France*

[4]*Department of Chemistry, University of Reading, Whiteknights, Reading, Berkshire RG6 6AD, United Kingdom*

(Received 28 September 2010; revised manuscript received 18 November 2010; published 21 January 2011)

$Zn(CN)_2$ and $Ni(CN)_2$ are known for exhibiting anomalous thermal expansion over a wide temperature range. The volume thermal expansion coefficient for the cubic, three-dimensionally connected material, $Zn(CN)_2$, is negative ($\alpha_V = -51 \times 10^{-6}$ K^{-1}) while for $Ni(CN)_2$, a tetragonal material, the thermal expansion coefficient is negative in the two-dimensionally connected sheets ($\alpha_a = -7 \times 10^{-6}$ K^{-1}), but the overall thermal expansion coefficient is positive ($\alpha_V = 48 \times 10^{-6}$ K^{-1}). We have measured the temperature dependence of phonon spectra in these compounds and analyzed them using *ab initio* calculations. The spectra of the two compounds show large differences that cannot be explained by simple mass renormalization of the modes involving Zn (65.38 amu) and Ni (58.69 amu) atoms. This reflects the fact that the structure and bonding are quite different in the two compounds. The calculated pressure dependence of the phonon modes and of the thermal expansion coefficient, α_V, are used to understand the anomalous behavior in these compounds. Our *ab initio* calculations indicate that phonon modes of energy ~2 meV are major contributors to negative thermal expansion (NTE) in both compounds. The low-energy modes of ~8 and 13 meV also contribute significantly to the NTE in $Zn(CN)_2$ and $Ni(CN)_2$, respectively. The measured temperature dependence of the phonon spectra has been used to estimate the total anharmonicity of both compounds. For $Zn(CN)_2$, the temperature-dependent measurements (total anharmonicity), along with our previously reported pressure dependence of the phonon spectra (quasiharmonic), is used to separate the explicit temperature effect at constant volume (intrinsic anharmonicity).

DOI: 10.1103/PhysRevB.83.024301 PACS number(s): 78.70.Nx, 63.20.−e, 65.40.−b

I. INTRODUCTION

The discovery of anomalous thermal expansion in framework solids is of fundamental scientific interest and may find application in fabricating technological materials, in particular for the optical and electronics industries. Besides oxide-based materials,[1,2] anomalous thermal expansion behavior has been observed in molecular framework materials containing linear diatomic bridges such as cyanide anions.[3–6] Recent x-ray diffraction measurements have shown[6] that the hexagonal materials, $Ag_3Co(CN)_6$ and $Ag_3Fe(CN)_6$, exhibit exceptionally large ("colossal") positive thermal expansion (PTE) along the a direction ($\alpha_a = +140 \times 10^{-6}$ K^{-1}) and negative thermal expansion (NTE) along the c direction ($\alpha_c = -125 \times 10^{-6}$ K^{-1}). These thermal expansion coefficients are an order of magnitude larger than those observed in any other material. Even simple cyanides such as $Zn(CN)_2$ are reported[5] to have an isotropic NTE coefficient ($\alpha_V = -51 \times 10^{-6}$ K^{-1}), which is twice as large as that of ZrW_2O_8.[1] However, when Zn is substituted by Ni, a layered compound, $Ni(CN)_2$, is produced,[3] which has NTE in two dimensions ($\alpha_a = -7 \times 10^{-6}$ K^{-1}) combined with a very large positive (PTE) coefficient ($\alpha_c = 61.8 \times 10^{-6}$ K^{-1}) in the third dimension perpendicular to the layers, to yield a large overall volume thermal expansion ($\alpha_V = 48.5 \times 10^{-6}$ K^{-1}).

It has been proposed from pair distribution function (PDF) analysis of the structural data collected using high-energy x rays that NTE in $Zn(CN)_2$ is induced by an average increase of the transverse thermal amplitude of the motion of bridging C/N atoms, away from the body diagonal.[7] Further, an investigation using *ab initio* calculations[8] of the geometry and electronic structure of $Zn(CN)_2$ shows that the naturally stiff C≡N bond is paired with weak Zn-C/N bonds. This type of bonding allows large transverse thermally excited motions of the bridging C/N atoms to occur in (*M*-CN-*M*) bridges within metal-cyanide frameworks. Structural studies[9] of $Zn(CN)_2$ show that two different models having a cubic symmetry with space group $Pn3m$ (disordered model) and $P43m$ (ordered model) give equally good accounts of the diffraction data. The ordered structure (Fig. 1) consists of a ZnC_4 tetrahedron (at the center of the cell) linked to four neighboring ZnN_4 tetrahedra (at the corners of the cell) with CN groups along four of the body diagonals. In the x-ray diffraction modeling of the disordered structure, atomic sites are given 50:50 C:N occupancy. Such models cannot be used for *ab initio* calculations, where sites can contain only one type of atom, thus restricting the space group to $P43m$.

$Ni(CN)_2$ is fundamentally different from $Zn(CN)_2$ in that it forms a layered structure with average tetragonal symmetry. Nickel cyanide has a long-range ordered structure in two dimensions (a-b plane) (Fig. 2) but a high degree of stacking disorder in the third dimension. The relationship between neighboring layers is defined, but there is a random element to the relationship between next-nearest neighbors. A crystallographic model in $P4_2/mmc$ (Ref. 3) reproduces the structure well and the disorder in the stacking is dealt with more comprehensively in the paper by Goodwin *et al.*[4] The gridlike layers (a-b plane) (Fig. 2) consist of NiC_4 square-planar units (as shown at the center of the figure), which are linked by vertex sharing to four neighboring NiN_4 square-planar units (shown at the corners of the figure) with the resultant CN groups

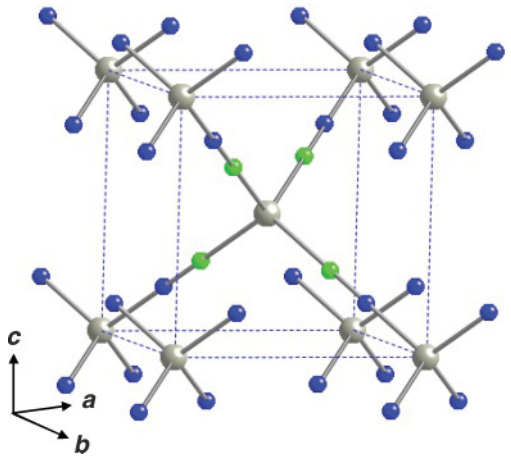

FIG. 1. (Color online) The structure of $Zn(CN)_2$ in $P43m$. Key: Zn, gray spheres; C, green spheres; N, blue spheres.

along the diagonals in the *a*-*b* plane. The covalent bonding within the layers is much stronger than the van der Waals' bonding between the layers, and it is this component that is studied in the calculations presented here, where effectively isolated $Ni(CN)_2$ layers are considered. Nickel cyanide shows anisotropic thermal behavior. Although the dimensions of its square gridlike layers (*a*-*b* plane) decrease with increasing temperature, this decrease is accompanied by a length increase along the *c* direction, giving an overall positive thermal expansion.

As already mentioned above, motions at right angles to the atomic and/or molecular bonds are identified as the principal cause of anomalous thermal expansion in framework compounds. Such motions are necessarily connected with transverse vibrations. For the amplitudes of motion to be large, the corresponding vibrations should be low in energy. That low-energy phonon modes play an important role in anomalous thermal expansion has been demonstrated by previous work[10–15] on ZrW_2O_8 and HfW_2O_8. In the case of $Zn(CN)_2$, time-of-flight inelastic neutron scattering measurements from powdered samples[16] indicate the existence of dispersionless modes at ∼2 meV (∼16 cm^1). To produce thermal expansion,

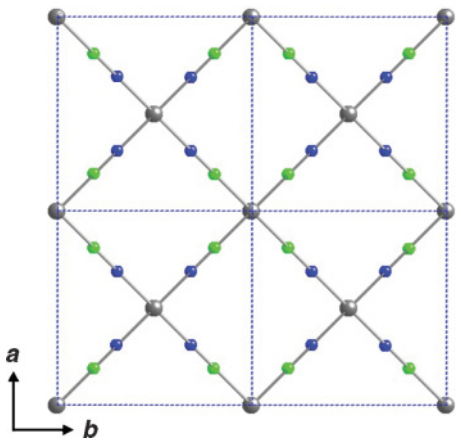

FIG. 2. (Color online) The structure of part of one layer of $Ni(CN)_2$ with D_{4h} symmetry. Key: Ni, gray spheres; C, green spheres; N, blue spheres.

vibrations not only have to be of large amplitude, but also have to be anharmonic in nature. To this end, we have recently investigated the anharmonicity of phonons in $Zn(CN)_2$ (Ref. 17) by employing a high-pressure inelastic neutron scattering technique. In this article we extend these investigations by including the temperature dependence of the $Zn(CN)_2$ spectra, together with a comparison with $Ni(CN)_2$. The analysis of the experiments is performed with the help of state-of-the-art *ab initio* lattice dynamical calculations. In this way we obtain a clear and detailed insight into the phonon mechanisms responsible for thermal expansion in $Zn(CN)_2$ and $Ni(CN)_2$.

II. EXPERIMENTAL

A $Zn(CN)_2$ (∼98.0% pure) polycrystalline sample was obtained from Aldrich, USA. The $Ni(CN)_2 \cdot 1.5H_2O$, purchased from Alfa Aesar, was dried under vacuum at room temperature for 12 h, reground, and then dried under vacuum at 200 °C for 3 weeks. Powder x-ray diffraction showed that the hydrated nickel cyanide had been completely converted to anhydrous nickel cyanide and that $Ni(CN)_2$ was the only crystalline phase present. The IR spectrum of $Ni(CN)_2$, collected using a Perkin Elmer 100 Fourier transform infrared (FTIR) spectrometer with a Universal ATR sampling accessory, confirmed that the material was fully dehydrated. The Raman spectrum was collected on a Renishaw InVia Raman microscope.

The inelastic neutron scattering experiments were performed using the IN6 time-of-flight spectrometer at the Institut Laue-Langevin (ILL), in Grenoble, France. The temperature-dependent measurements were performed on ∼10 g of polycrystalline samples of $Zn(CN)_2$ and $Ni(CN)_2$. The samples were placed in a cryostat inside sealed thin-slab aluminum containers mounted at 45° with respect to the incident neutron beam. The high-resolution data for $Zn(CN)_2$ and $Ni(CN)_2$ were measured at several temperatures from 300 to 160 K. The measurements were performed in the neutron-energy gain inelastic focusing mode with an incident neutron wavelength of 5.12 Å (3.12 meV) and 4.14 Å (4.77 meV) for $Zn(CN)_2$ and $Ni(CN)_2$, respectively,. The elastic energy resolution of the spectrometer is 0.20 meV for $\lambda = 5.12$ Å and 0.30 meV for $\lambda = 4.14$ Å in the inelastic focusing mode. The spectrometer is equipped with a large detector bank covering a wide range of scattering angle (10°–115°).

In the incoherent one-phonon approximation, the phonon density of states[18] is related to the measured scattering function $S(Q,E)$, as observed in the neutron experiments by

$$g^{(n)}(E) = A\left\langle \frac{e^{2W_k(Q)}}{Q^2} \frac{E}{n(E,T) + \frac{1}{2} \pm \frac{1}{2}} S(Q,E) \right\rangle, \quad (1)$$

$$g^n(E) = B \sum_k \left(\frac{4\pi b_k^2}{m_k} \right) g_k(E), \quad (2)$$

where the + or − signs correspond to energy loss or gain of the neutrons, respectively, and $n(E,T) = [\exp(E/k_BT) - 1]^{-1}$. A and B are normalization constants and b_k,m_k, and $g_k(E)$ are, respectively, the neutron scattering length, mass, and partial density of states of the kth atom in the unit cell. The quantity within $\langle \cdots \rangle$ represents an appropriate average over all Q values

TABLE I. Fractional atomic coordinates used to generate the $Ni(CN)_2$ layers within the tetragonal space group $P4$ for $Ni(CN)_2$. a=b=6.869 00 Å and c=6.405 00 Å.

Ni	0.0	0.0	0.0
Ni	0.5	0.5	0.0
C	0.1909	0.1909	0.
N	0.3091	0.3091	0.0

at a given energy. $2W(Q)$ is the Debye-Waller factor. The weighting factors $\frac{4\pi b_k^2}{m_k}$ for each atom type in the units of barns/amu are as follows: Zn: 0.063; Ni: 0.315; C: 0.462; and N: 0.822 calculated from the neutron scattering lengths found in Ref. 19.

III. LATTICE DYNAMICAL CALCULATIONS

Ab initio calculations were performed using the projector-augmented wave (PAW) formalism[20] of the Kohn-Sham discrete Fourier transform (DFT) (Refs. 21 and 22) at the generalized gradient approximation level (GGA), implemented in the Vienna *ab initio* simulation package (VASP).[23,24] The GGA was formulated by the Perdew-Burke-Ernzerhof (PBE) (Refs. 25 and 26) density functional. The Gaussian broadening technique was adopted and all results are well converged with respect to k mesh and energy cutoff for the plane-wave expansion. The partially relaxed (only coordinates are optimized) ordered structures of $Zn(CN)_2$ and $Ni(CN)_2$ were used for the lattice dynamical calculations and related properties. For $Zn(CN)_2$, the available structure having the cubic space group ($P43m$ (215), $[T_d^1]$) is considered.[9] For $Ni(CN)_2$, a periodic model system is used (Table I) to generate the layers within the tetragonal space group ($P4$ (75) $[C_4^1]$).[4] This model for $Ni(CN)_2$ is an approximation of the real situation as the interlayer spacing used is double that found in the actual material. Such a model results in no interaction between the layers. However, the model can be used to reproduce most features of the Raman spectrum, the phonon density of states (DOS) and, in addition, can be used to investigate the in-plane negative thermal expansion.

In the lattice dynamics calculations, in order to determine all interatomic force constants, the supercell approach has been adopted.[27] For both $Ni(CN)_2$ and $Zn(CN)_2$, ($2a$,$2b$,$2c$) super cells containing 16 formula units (80 atoms) were constructed. Total energies and interatomic forces were calculated for the 20 structures generated for $Ni(CN)_2$ and for the eight structures, generated for $Zn(CN)_2$, by displacement of the four symmetry inequivalent atoms present in both systems along the three Cartesian directions ($\pm x$, $\pm y$, and $\pm z$). DOS, phonon dispersion relations (PDR), and Raman active modes and/or frequencies were extracted in subsequent calculations using the Phonon software.[28]

IV. RESULTS AND DISCUSSION

A. Phonon density of states and dispersion relation

The measured temperature dependence of the phonon spectra for $Zn(CN)_2$ and $Ni(CN)_2$ are shown in Figs. 3 and 4, respectively. Differential scanning calorimetric measurements[29] for $Zn(CN)_2$ show an anomaly at ~250 K. The phonon spectra for $Zn(CN)_2$ (Fig. 3) have been measured at 180, 240, 270, and 320 K. These measurements show a visible change in the phonon spectra at ~50 meV with a change of temperature from 240 to 270 K that matches the temperature of the anomaly in the calorimetric measurements. All the observed features for $Zn(CN)_2$ are well reproduced computationally (Fig. 3), especially the low-energy peak at ~2 meV.

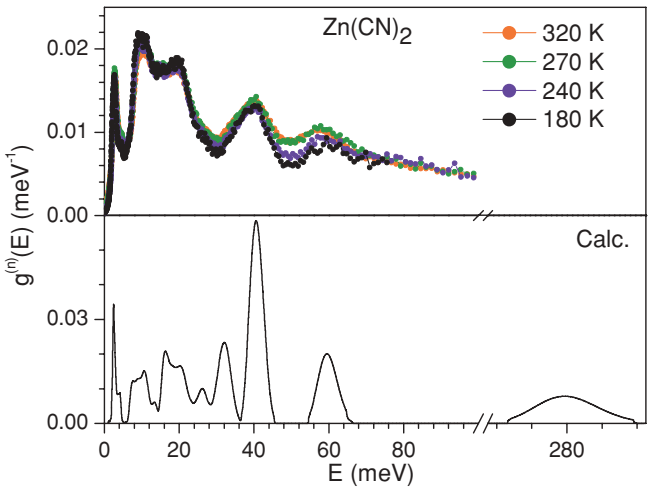

FIG. 3. (Color online) The temperature dependence of the phonon spectra for $Zn(CN)_2$. The phonon spectra are measured with an incident neutron wavelength of 5.12 Å using the IN6 spectrometer at ILL. The calculated phonon spectra from *ab initio* calculations are also shown. The calculated spectra have been convoluted with a Gaussian of FWHM of 10% of the energy transfer in order to describe the effect of energy resolution in the experiment carried out using the IN6 spectrometer.

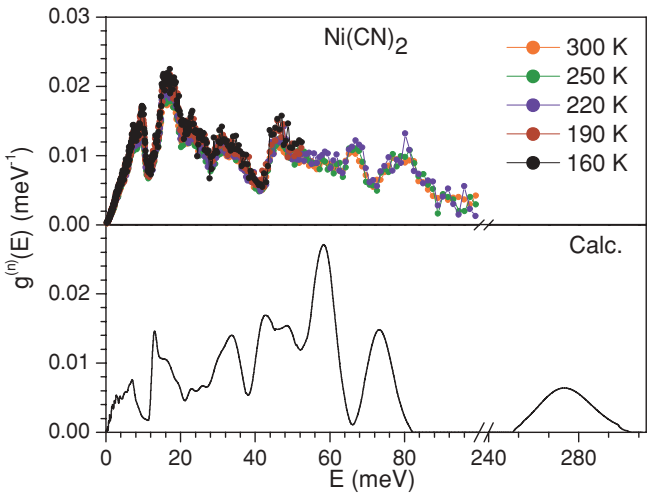

FIG. 4. (Color online) The temperature dependence of the phonon spectra for $Ni(CN)_2$. The phonon spectra are measured with an incident neutron wavelength of 4.14 Å using the IN6 spectrometer at ILL. The calculated phonon spectra from *ab initio* calculations are also shown. The calculated spectra have been convoluted with a Gaussian of FWHM of 10% of the energy transfer in order to describe the effect of energy resolution in the experiment carried out using the IN6 spectrometer.

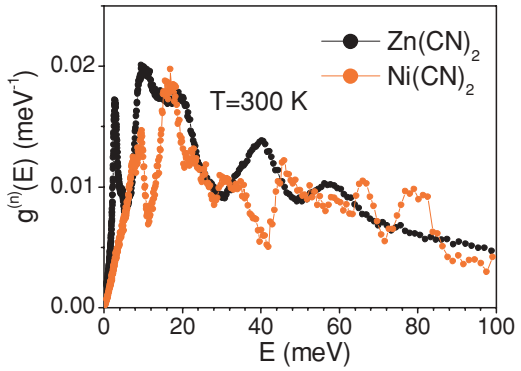

FIG. 5. (Color online) Comparison of the experimental phonon spectra for $Zn(CN)_2$ and $Ni(CN)_2$.

The experimental phonon spectrum of $Ni(CN)_2$ (Fig. 4) shows several well-pronounced vibration bands that do not show any significant temperature dependence. The calculated positions of these bands are in good agreement with the experimental data while there are slight differences in the intensities. This is probably owing to the fact that the interlayer interactions in $Ni(CN)_2$ have not been included. As we do neglect the interlayer coupling, the modes along the stacking axis have very low energies. All these modes are included in the calculated DOS that we have shown in Fig. 4. This explains the extra weight in the calculated DOS at low energies.

The comparison of the phonon spectra of $Zn(CN)_2$ and $Ni(CN)_2$ shows (Fig. 5) that there are pronounced differences. The cutoff energy for the external modes in $Zn(CN)_2$ and $Ni(CN)_2$ is at ∼65 and 90 meV, respectively. The calculated partial DOS show that the contributions from Zn and Ni in $Zn(CN)_2$ and $Ni(CN)_2$ (Fig. 6) extend up to 60 and 75 meV, respectively. These differences cannot be explained obviously by a simple mass renormalization of the modes involving Zn (65.38 amu) and Ni (58.69 amu) atoms. They thus imply that the strength and may be the character of bonding is different in

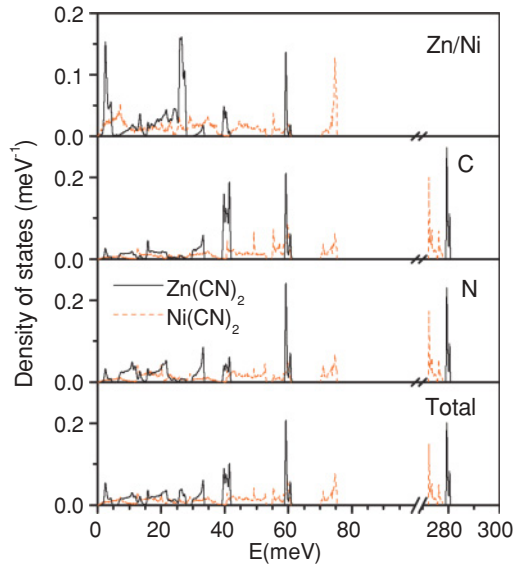

FIG. 6. (Color online) The calculated partial density of states for the various atoms in $Zn(CN)_2$ and $Ni(CN)_2$.

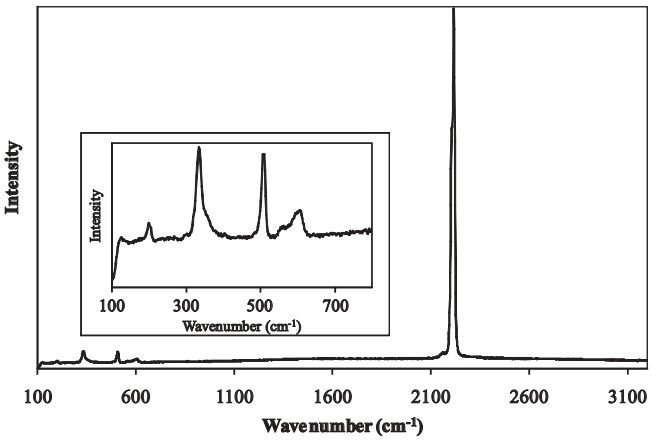

FIG. 7. Raman spectrum of $Ni(CN)_2$. Inset shows enlargement of the low-wave number region.

both systems. Our inelastic scattering data show that the first low-energy band in the Zn compound is at 2 meV, while in the Ni compound this band is at 10 meV.

The structures of $Zn(CN)_2$ and $Ni(CN)_2$ yield 30 phonon modes for each wave vector. The measurements of Raman modes for $Zn(CN)_2$ are reported in Ref. 30. For $Ni(CN)_2$ no such data are available in the literature to our knowledge. Our Raman measurements on $Ni(CN)_2$ are shown in Fig. 7. Specifically the $\nu_{C\equiv N}$ region for both the Raman and infrared spectra of $Ni(CN)_2$ is shown in Fig. 8. The presence of two $\nu_{C\equiv N}$ absorptions in the Raman and one in the infrared spectrum (Fig. 8) is consistent with D_{4h} symmetry.

The comparison between the experimental and calculated zone-center modes for $Zn(CN)_2$ (Ref. 30) and $Ni(CN)_2$ is given in Tables II and III, respectively. The agreement is very close in each case. Reference 4 reported five dispersionless phonon modes below 1.0 THz (4.136 meV) arising from motions of a single $Ni(CN)_2$ layer, as obtained from reverse Monte Carlo fitting of total neutron diffraction data. However, our calculations for $Ni(CN)_2$ produces the lowest optic mode at 99 cm^{-1} (∼3 THz, ∼12.3 meV) (Fig. 9), in agreement with the Raman data (Table III).

The calculated phonon dispersion curves for $Zn(CN)_2$ are shown in Fig. 9. We notice a remarkable flat phonon dispersion

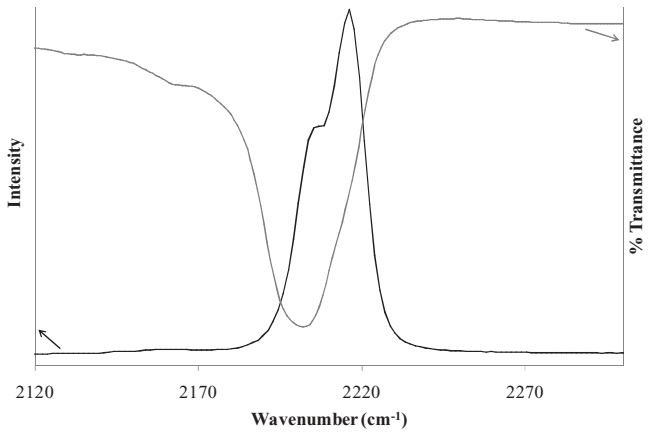

FIG. 8. The $\nu_{C\equiv N}$ region of the Raman (black) and infrared (gray) spectra for $Ni(CN)_2$.

TABLE II. *Ab initio* calculated (Calc.) and observed (Exp.) (Ref. 30) Raman and IR frequencies (cm^{-1}) for $Zn(CN)_2$. Irrep., Type, and M stand for irreducible representation, type of the mode, and multiplicity, respectively. R, RI, and S indicate if the mode is Raman active or is both Raman and IR active or optically inactive, respectively. The point group symmetry is T_d^1. The experimental Raman and IR frequencies are taken from Table I of Ref. 30.

Calc.	59	173	178	204	240	330	336	476	481	2251	2261
Exp.			178	216		343	339	461		2218	2221
Irrep.	T_1	E	T_2	T_2	T_1	T_2	E	A_1	T_2	T_2	A_1
Type	S	R	RI	RI	S	RI	R	RI	R	RI	R
M	3	2	3	3	3	3	2	3	1	3	1

sheet of the two lowest-energy acoustic modes at ∼2 meV. These flat modes give rise to the observed first peak in the DOS at ∼2 meV. Further flat phonon dispersion sheets are found at relatively high energies of ∼25, 30, 40, and 60 meV (Fig. 9), providing the other well isolated bands in the DOS (Fig. 3). The calculated dispersion relation for $Ni(CN)_2$ (Fig. 9) is quite different as compared to $Zn(CN)_2$. As explained in Sec. III, the calculations for $Ni(CN)_2$ are carried out with the layers separated, which is different from the real situation. Further, we find that at zone boundary the acoustic modes extend up to 10 meV. The flattening of acoustic modes at ∼10 meV gives rise to the first peak in the DOS (Figs. 4 and 5) of $Ni(CN)_2$. The large difference in the energies of acoustic modes between the compounds indicates that bonding is quite different in both compounds. Further, the flat phonon dispersion sheets at ∼18, 30, 45, 60, and 75 meV give rise to the isolated peaks in the DOS of $Ni(CN)_2$. The Bose-factor corrected $S(Q,E)$ plots for $Zn(CN)_2$ and $Ni(CN)_2$ at 180 and 160 K, respectively, are shown in Fig. 10. The figure clearly shows the presence of flat acoustic modes at 2 meV in the $S(Q,E)$ plot of $Zn(CN)_2$, while for $Ni(CN)_2$ the acoustic modes extend up to ∼10 meV.

In case of $Ni(CN)_2$ the acoustic dispersion within the sheets for the transverse branches possesses in the calculation an anomalous dispersion. The curves turn upward instead of downward with respect to increasing q. Naturally, the anomalous dispersion could become normal by including the interplanar coupling. On the other hand, the measured DOS (Fig. 4) seems to be linear. This would be compatible with an anomalous dispersion. The fact that we do not see any soft modes in $S(Q,E)$ (Fig. 10) demonstrates that the interplanar coupling is certainly not negligible. If this was the case, then soft modes along the stacking direction would

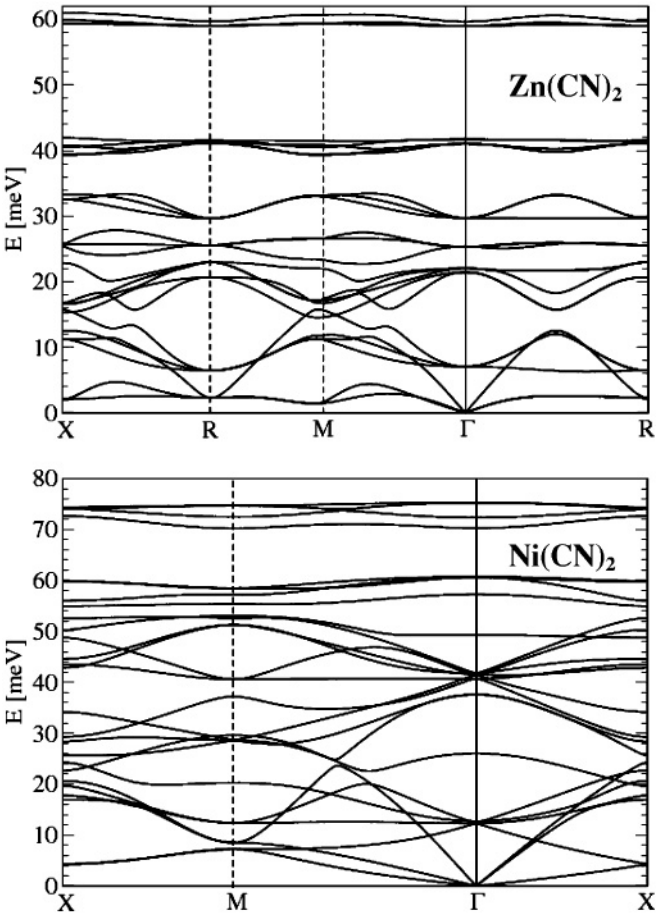

FIG. 9. The calculated phonon dispersion curves for $Zn(CN)_2$ and $Ni(CN)_2$. The Bradley-Cracknell notation is used for the high-symmetry points along which the dispersion relations are obtained. $Zn(CN)_2$: $\Gamma = (0,0,0)$, $X = (1/2,0,0)$, $M = (1/2,1/2,0)$, and $R = (1/2,1/2,1/2)$. $Ni(CN)_2$: $\Gamma = (0,0,0)$, $X(1/2,0,0)$, and $M(1/2,1/2,0)$. In order to expand the y scale, the sets of four and three dispersionless modes, respectively, in $Zn(CN)_2$ and $Ni(CN)_2$ owing to the cyanide stretch at ∼280 meV are not shown.

TABLE III. *Ab initio* calculated (Calc.) and observed (Exp.) Raman and IR frequencies (cm^{-1}) for $Ni(CN)_2$. Irrep, Type, and M stand for irreducible representation, type of the mode, and multiplicity, respectively. R and RI indicate if the mode is Raman active or is both Raman and IR active, respectively. The point group symmetry is C_4^1, thus all IR are Raman active. A and E Irreps. (polar modes) are also IR, with polarizations lying along the z axis and in the xy plane, respectively. The B modes are Raman active only.

Calc.	99	100	103	210	303	328	333	334	335	337
Exp.				200				334 (broad)		
Irrep.	E	A	A	B	E	E	A	A	B	E
Type	RI	RI	RI	R	RI	RI	RI	RI	R	RI
M	2	1	1	1	2	2	1	1	1	2
Calc.	397	461	489	490	566	583	606	2196	2205	2238
Exp.				508	561	604	607	2202	2206	2215
Irrep.	B	A	E	B	B	A	E	E	B	A
Type	R	RI	RI	R	R	RI	RI	RI	R	RI
M	1	1	2	1	1	1	2	2	1	1

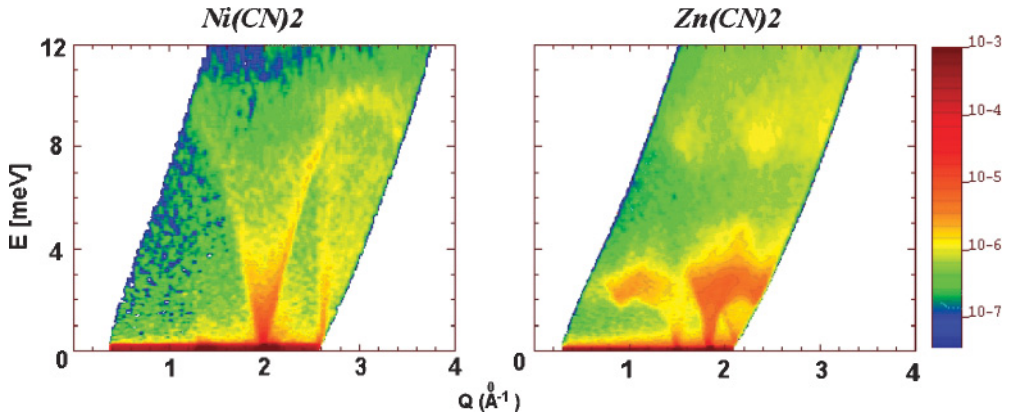

FIG. 10. (Color online) The experimental Bose-factor corrected $S(Q,E)$ plots for $Zn(CN)_2$ and $Ni(CN)_2$ at 180 and 160 K, respectively. The values of $S(Q,E)$ are normalized to the mass of the sample in the beam. For clarity, a logarithmic representation is used for the intensities. The measurements for $Zn(CN)_2$ and $Ni(CN)_2$ were performed with an incident neutron wavelength of 5.12 Å (3.12 meV) and 4.14 Å (4.77 meV), respectively.

be inevitable. Therefore, the contraction of the plane certainly should influence the physics along the stacking axis.

B. Grüneisen parameters and thermal expansion

The calculation of thermal expansion is carried out using the quasiharmonic approximation. Each mode of energy E_i contributes to the volume thermal expansion coefficient[31] given by $\alpha_V = \frac{1}{BV}\Sigma_i \Gamma_i C_{Vi}(T)$, where V is the unit cell volume, B is the bulk modulus, Γ_i $(= -\partial \ln E_i/\partial \ln V)$ are the mode Grüneisen parameters, and C_{Vi} is the specific-heat contributions of the phonons in state i $(= \mathbf{q}_j)$ of energy E_i. Our published high-pressure inelastic neutron scattering experiments[17] on polycrystalline samples of $Zn(CN)_2$ enabled us to estimate the energy dependence of the ratios $\frac{\Gamma_i}{B}$ at 165 and 225 K. The measurements show that the $\frac{\Gamma_i}{B}$ values are nearly the same at 165 and 225 K. The thermal expansion coefficient derived from the phonon data[17] is in good agreement with that obtained from diffraction measurements.[5]

In order to estimate theoretically the volume thermal expansion coefficient, we have calculated the Grüneisen parameters based on the DOS at two different unit-cell

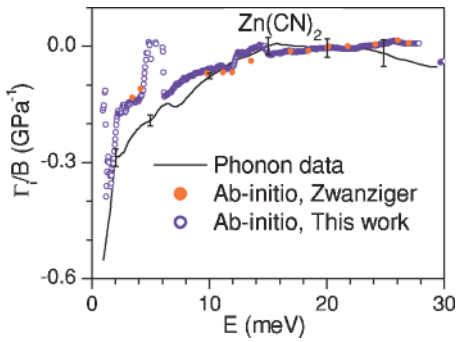

FIG. 11. (Color online) The comparison between the experimental and calculated $\frac{\Gamma_i}{B}$ plotted as a function of phonon energy E. The $\frac{\Gamma_i}{B}$ values derived from *ab initio* calculations from Ref. 33 are shown by closed circles. The $\frac{\Gamma_i}{B}$ values represent the average over the whole Brillouin zone.

volumes. In addition to the phonon spectra at the experimental cell volumes, we calculated the phonon spectra using the lattice parameters reduced by 0.2%, together with reoptimized atomic positions. The calculation of the bulk modulus, B, was then accomplished by determining the total energy of the materials as a function of unit-cell volumes and fitting them to a Birch equation of state.[32] We obtain values for B of 84.1 GPa for $Zn(CN)_2$ and 63.4 GPa for $Ni(CN)_2$.

The calculated $\frac{\Gamma_i}{B}$ for $Zn(CN)_2$ and $Ni(CN)_2$ are shown in Figs. 11 and 12(a), respectively. The modes up to 15 meV show negative $\frac{\Gamma_i}{B}$, with the low-frequency modes at ∼2 meV for $Zn(CN)_2$ showing the largest negative $\frac{\Gamma_i}{B}$. The calculated $\frac{\Gamma_i}{B}$ for $Zn(CN)_2$ (Fig. 11) are in very good agreement with the values obtained from our high-pressure inelastic neutron scattering measurements and for higher-frequency modes with the *ab initio* calculations done by Zwanziger.[33] The calculated temperature dependence of the volume thermal expansion coefficient derived from these $\frac{\Gamma_i}{B}$ values compares very well with those derived from our phonon data [Fig. 13(a)]. These values for $Zn(CN)_2$ can be used to calculate the volume expansion, and both are in good agreement with the corresponding value obtained from diffraction data[5] [Fig. 13(b)]. The *ab initio* calculations by Zwanziger[33] give a thermal expansion coefficient of -12×10^{-6} K^{-1} at 5 K, in agreement with the experimental data. However, Zwanziger[33] did not report Grüneisen parameters of modes below 3 meV, or a detailed temperature dependence of α_V. Note that the value of α_V changes to -51×10^{-6} at 300 K.

$Ni(CN)_2$ shows two-dimensional NTE (Ref. 3) in the a-b plane with $\alpha_a = -6.5 \times 10^{-6}$ K^{-1}. The large positive expansion[3] along c ($\alpha_c = 61.8 \times 10^{-6}$ K^{-1}) results in an increase in volume with temperature ($\alpha_V = 48.5 \times 10^{-6}$ K^{-1}). The experimental $\frac{\Gamma_i}{B}$ values are not available, however, these values should be positive for positive α_V. We have carried out *ab initio* calculations for $Ni(CN)_2$ on what are effectively isolated sheets. By separating the sheets, we are able to employ $P4$ symmetry and achieve a great saving in computational resource. Structures with the sheets at the correct separation and alignment can be described only in $P1$. This is the case because, in contrast to the modeling of diffraction patterns,

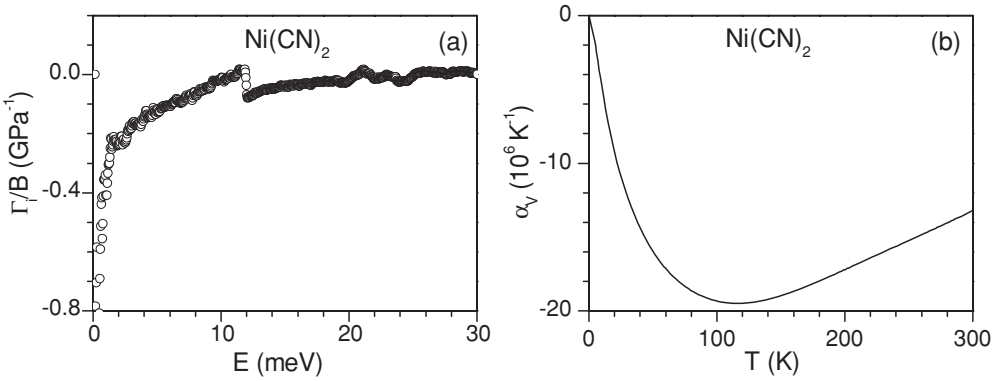

FIG. 12. (a) The calculated $\frac{\Gamma_i}{B}$ and (b) volume thermal expansion coefficient (α_V) derived for $Ni(CN)_2$ from *ab initio* calculations.

where an average C/N atom can be employed, in *ab initio* calculations discrete C or N atoms must occupy any individual atomic site. The use of $P1$ symmetry would be prohibitively expensive in computing time in *ab initio* calculations of the type employed here. Attempts to introduce stacking disorder of the type found in $Ni(CN)_2$ into the modeling would present additional computing costs.

We find that such a model gives negative $\frac{\Gamma_i}{B}$ [Fig. 12(a)] for $Ni(CN)_2$. The calculated average α_V [Fig. 12(b)] in the 100–300 K range is -16.5×10^{-6} K^{-1}, which gives a linear $\alpha_L = -5.5 \times 10^{-6}$ K^{-1} and compares excellently with the α_a value of -6.5×10^{-6} K^{-1} from diffraction experiments.[5] Unfortunately, our modeling produces no quantitative information on the third dimension because we have modeled effectively isolated sheets. A qualitative explanation of the overall positive expansion of this system is that, as these layers contract in the *a-b* plane, they expand into the third dimension, pushing the layers apart, as suggested in Hibble *et al.*[3] The weak interactions between the layers mean that expansion in this direction is easy and explains the overall PTE in this system.

The estimated $\frac{\Gamma_i}{B}$ values (Fig. 11) from *ab initio* calculations have been used to estimate the contribution of the various phonons to the thermal expansion (Fig. 14) as a function of phonon energy in $Zn(CN)_2$ at 165 K. Previously, we estimated this contribution from our experimental $\frac{\Gamma_i}{B}$ obtained from high-pressure phonon data.[17] We find that these estimates from experiment and *ab initio* calculation as given in Fig. 14 are quite close. The maximum negative contribution to α_V stems from the low-energy modes at ∼2.5 meV. Similarly for $Ni(CN)_2$, we find (Fig. 14) that maximum contribution to NTE is also from phonon modes of an approximate energy of 2.5 meV. This maximum strength appears well below the first maximum in the DOS (Fig. 4), which is found at 4 meV. The low-energy modes of ∼8 and 13 meV also contribute significantly (Fig. 14) to the NTE in $Zn(CN)_2$ and $Ni(CN)_2$, respectively.

NTE has been observed in a large number of polyhedral network compounds, e.g., AW_2O_8 (A = Zr, Hf), ZrV_2O_7, M_2O (M = Cu, Ag), ReO_3, etc. The phonon softening corresponding to large negative Grüneisen parameters $\Gamma(E)$ leads to NTE in all these compounds. The negative $\Gamma(E)$ and the nature of phonons have been calculated previously using model calculations based on a shell model. The nature of phonons is found to be different in all these compounds. The librational and bending modes of ∼1.5–8.0 meV were found[14,15] to be responsible for large negative $\Gamma(E)$ in AW_2O_8 (A = Zr,Hf), whereas for ZrV_2O_7 the soft phonon[34] occur at an incommensurate wave vector. Soft-librational modes of the M_4O (M = Cu, Ag), tetrahedral units[35] are related to NTE in M_2O. In the case of ReO_3, the zone-boundary $M3$ mode softens[36] and leads to anomalous thermal behavior.

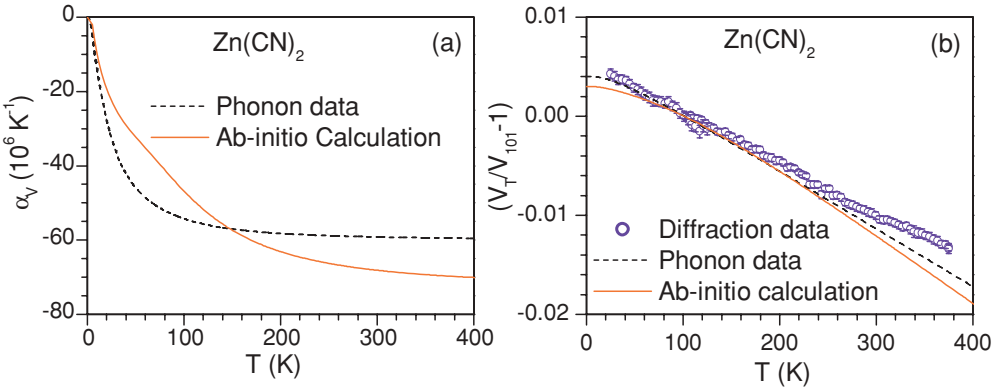

FIG. 13. (Color online) (a) The comparison between the volume thermal expansion coefficient (α_V) derived from the *ab initio* calculations and experimental $\frac{\Gamma_i}{B}$ values (Ref. 17) at 165 K. (b) The comparison between the volume thermal expansion derived from the present *ab initio* calculations (solid line), high-pressure inelastic neutron scattering experiment (Ref. 17) (dashed line), and that obtained using x-ray diffraction (Ref. 5) (open circles).

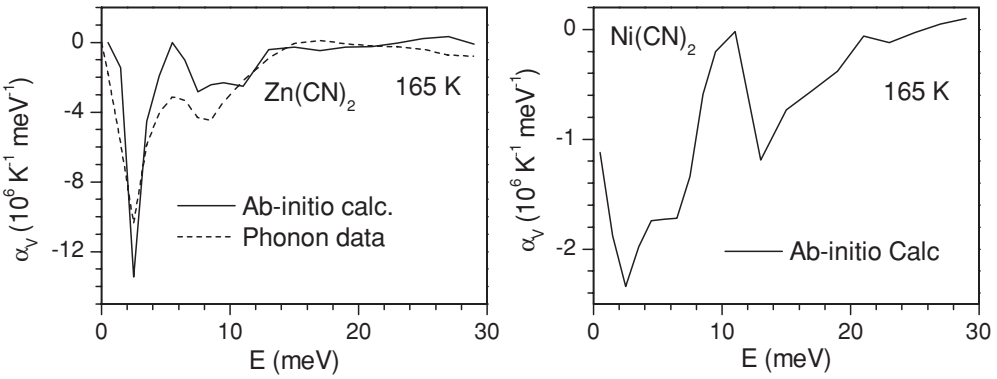

FIG. 14. The contribution of phonons of energy E to the volume thermal expansion coefficient (α_V) as a function of E at 165 K in $Zn(CN)_2$ and $Ni(CN)_2$. The contribution from phonons for $Zn(CN)_2$ is obtained from experimental $\frac{\Gamma_i}{B}$ as indicated in Ref. 17.

In order to determine the character of phonon modes in $Zn(CN)_2$ and $Ni(CN)_2$, we have calculated the mean squared displacements of various atoms, $\langle(u^2)\rangle$, arising from all phonons of energy E in the Brillouin zone, as follows:

$$\langle(u^2)_k\rangle = \int \left(n + \frac{1}{2}\right) \frac{\hbar}{m_k \omega_k} g(\omega_k)\, d\omega_k, \qquad (3)$$

where $n = [\exp(\frac{\hbar\omega_k}{k_B T}) - 1]^{-1}$, and ω_k and m_k are the mode frequency and mass of the kth atom in the unit cell, respectively. The calculated partial DOS (Fig. 6) has been used for this calculation.

Figure 15 indicates equal amplitudes for all the atoms up to 5 meV in $Zn(CN)_2$ and 12 meV in $Ni(CN)_2$. The contributions from Zn and Ni atoms vanish above these energies. It is reasonable to conclude that the lowest bands without significant Zn contribution to the vibration amplitude correspond to rotational modes in $Zn(CN)_2$. The ZnC_4 and ZnN_4 rotational modes in $Zn(CN)_2$ are therefore found at lower energies (5–12 meV), in comparison to NiC_4 and NiN_4 (12–16 meV) rotational modes in $Ni(CN)_2$.

We have also plotted eigenvectors corresponding to low-energy zone-center and zone-boundary modes (Figs. 16 and 17). The mode assignments, phonon energies, and Grüneisen parameters are given in the figures. Examination of the calculated eigenvectors for the lowest-energy optic mode (symmetry T_1) at 7.3 meV in $Zn(CN)_2$ (Table II) shows that this mode arises from librational motions of ZnC_4 and ZnN_4 tetrahedra involving transverse motions of C and N atoms. The T_1 mode has a Γ value of -9.8. As shown above, modes with energies of $\sim$8 meV contribute significantly to NTE in $Zn(CN)_2$ (Fig. 14). However, Fig. 14 shows that modes of energy $\sim$2 meV make the most significant contributions to NTE in $Zn(CN)_2$. The zone-boundary modes of about 2 meV along (100), (110), and (111) are plotted in Fig. 16. At the zone boundary, eigenvectors have both real and imaginary components. We have plotted both these components separately. The actual atomic motion is a combination of both these components. We find that only the real part of the 1.94 meV mode along (100) shows librational motion (Fig. 16). All other modes show translational and bending motions. Our calculations show that zone-boundary modes along [100] and [110] have very large negative Γ values of -48.4 and -85.8, respectively, while the mode at the zone boundary along [111] has a very low negative Γ value of -0.7.

$Ni(CN)_2$ has three low-energy optic modes at $\sim$12.32 meV (E mode), 12.35 meV (A mode), and 12.77 meV (A mode) (Table III and Fig. 9). We find that only the A-type mode of energy 12.77 meV shows librational motion (Fig. 17). The other two zone-center modes (12.32 and 12.35 meV) as well as the zone-boundary modes (4.26–7.3 meV) involve (Fig. 17) translations of atoms along the c axis. The negative Γ values of all the three optic modes lie between -4.5 and -6.0, while zone-boundary modes along [100] have large negative Γ values

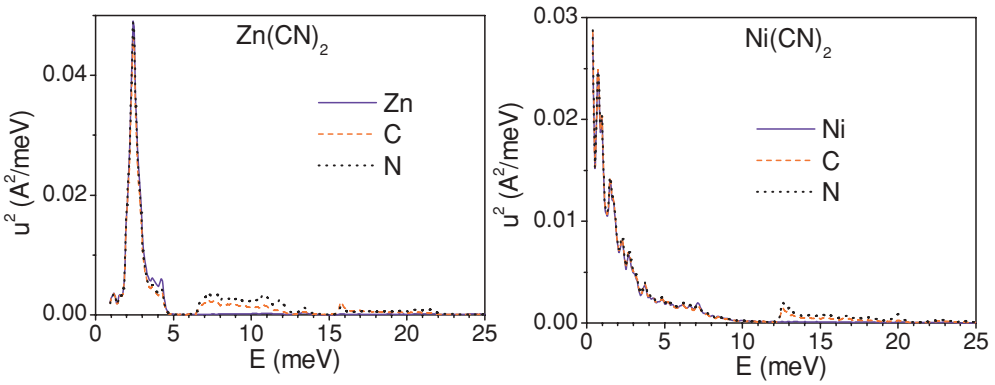

FIG. 15. (Color online) The calculated contribution to the mean squared amplitude of the various atoms arising from phonons of energy E at $T = 300$ K in $Zn(CN)_2$ and $Ni(CN)_2$.

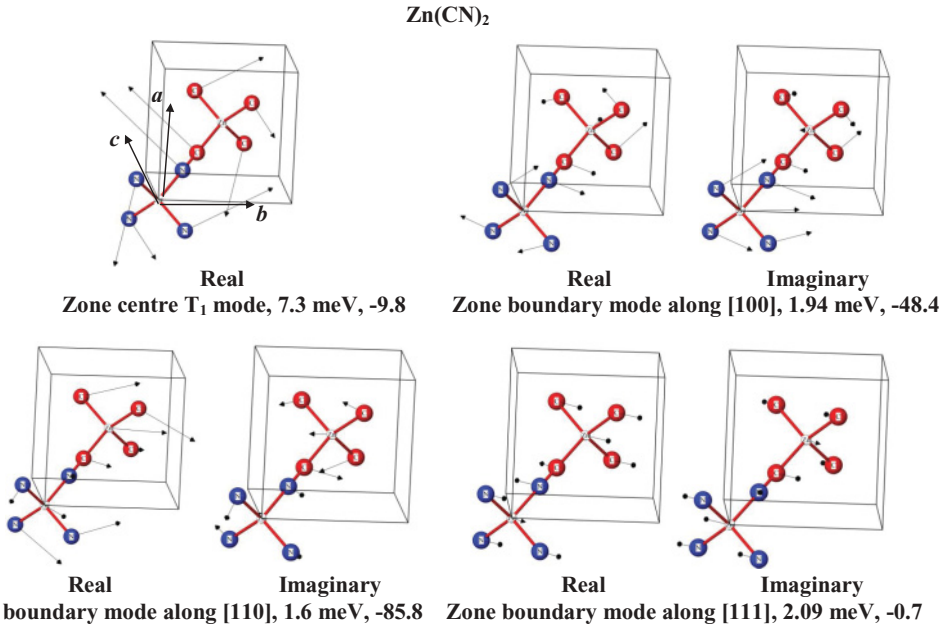

FIG. 16. (Color online) Polarization vectors of the zone-center and zone-boundary modes in $Zn(CN)_2$. For each mode the energy and Grüneisen parameter is indicated. The lengths of arrows are related to the displacements of the atoms. The absence of an arrow on an atom indicates that the atom is at rest. At the zone center, where the phase factor is zero, the eigenvectors have only real components. The numbers after the mode assignments give the phonon energies and Grüneisen parameters, respectively. Zone-boundary eigenvectors have both real and imaginary components. The actual displacements of atoms are a combination of both these components. Key: Zn, gray spheres; C, red spheres; N, blue spheres.

(~ -13.0) as compared to those along [110] (~ -5.3). The modes at $\sim$2 meV make the most significant contribution to NTE. As shown in Fig. 9, the 2 meV modes are largely acoustic in nature, which include the transverse motions to produce NTE in agreement with Chapman *et al.*[16]

C. Anharmonicity

The analysis presented here is important for understanding the anharmonic nature of phonons in these compounds. The change in phonon energies with temperature is owing to implicit as well as explicit anharmonicities. The implicit anharmonicity of phonons is owing to the change of the unit-cell volume and/or concomitant changes of structural parameters with temperature. The explicit anharmonicity includes changes in phonon frequencies owing to a large thermal amplitude of atoms. The temperature-dependent measurements (total anharmonicity) include both effects. The present measurements of phonon spectra along with the previously reported pressure dependence of the phonon spectra (implicit anharmonicity) can be used to separate[37] the temperature effect at constant volume (explicit or true anharmonicity) as

$$\left.\frac{dE_i}{dT}\right|_P = \left.\frac{\partial E_i}{\partial T}\right|_V + \left.\frac{\partial E_i}{\partial V}\right|_T \left.\frac{\partial V}{\partial T}\right|_P .$$

Using $\Gamma_i = -\frac{V}{E_i}\frac{\partial E_i}{\partial V}|_T$ and $\alpha = -\frac{1}{V}\frac{\partial V}{\partial T}|_P$, one obtains

$$\left.\frac{1}{E_i}\frac{dE_i}{dT}\right|_P = \left.\frac{1}{E_i}\frac{\partial E_i}{\partial T}\right|_V - \Gamma_i\alpha. \qquad (4)$$

Here the first term on the right-hand side is the true anharmonic (explicit) contribution, and the second the quasiharmonic (implicit) term. The left-hand-side term represents the total anharmonicity. The temperature dependence of phonon spectra has been used for estimating the total anharmonicity ($\frac{1}{E_i}\frac{dE_i}{dT}|_P$) of both compounds. For $Zn(CN)_2$, the $\frac{1}{E_i}\frac{dE_i}{dT}|_P$ values for phonons of energy E_i have been obtained using the cumulative distributions of the experimental data of phonon density of states at 180 and 240 K, while for $Ni(CN)_2$ the experimental data at 160 and 220 K have been used to obtain $\frac{1}{E_i}\frac{dE_i}{dT}|_P$.

As mentioned above, the temperature-dependent measurements give estimates of the total anharmonicity of phonons and include both the implicit and explicit effects. On increasing the temperature, the implicit anharmonicity results in a decrease of phonon frequencies for all materials, irrespective of their thermal expansion coefficients. However, explicit contribution may cause either an increase or decrease of phonon frequencies with increasing temperature. Finally, it is the net sum of the two components, which we have observed in the measurements and shown in Figs. 3 and 4. We find that for $Ni(CN)_2$ the phonon energies increase with an increase (Fig. 18) of temperature, hence the total anharmonicity ($\frac{1}{E_i}\frac{dE_i}{dT}|_P$) is positive. In particular, modes below 2 meV have a very large total anharmonicity. Because the implicit part would result in softening of modes with an increase of temperature, the hardening of modes with an increase of temperature gives us evidence for the large explicit anharmonic nature of phonons in $Ni(CN)_2$.

In the case of $Zn(CN)_2$ (Fig. 18), for modes below 2 meV, the total anharmonicity of phonons is negative, while it is positive for high-energy modes. Because the implicit part causes a decrease of phonon frequencies with an increase

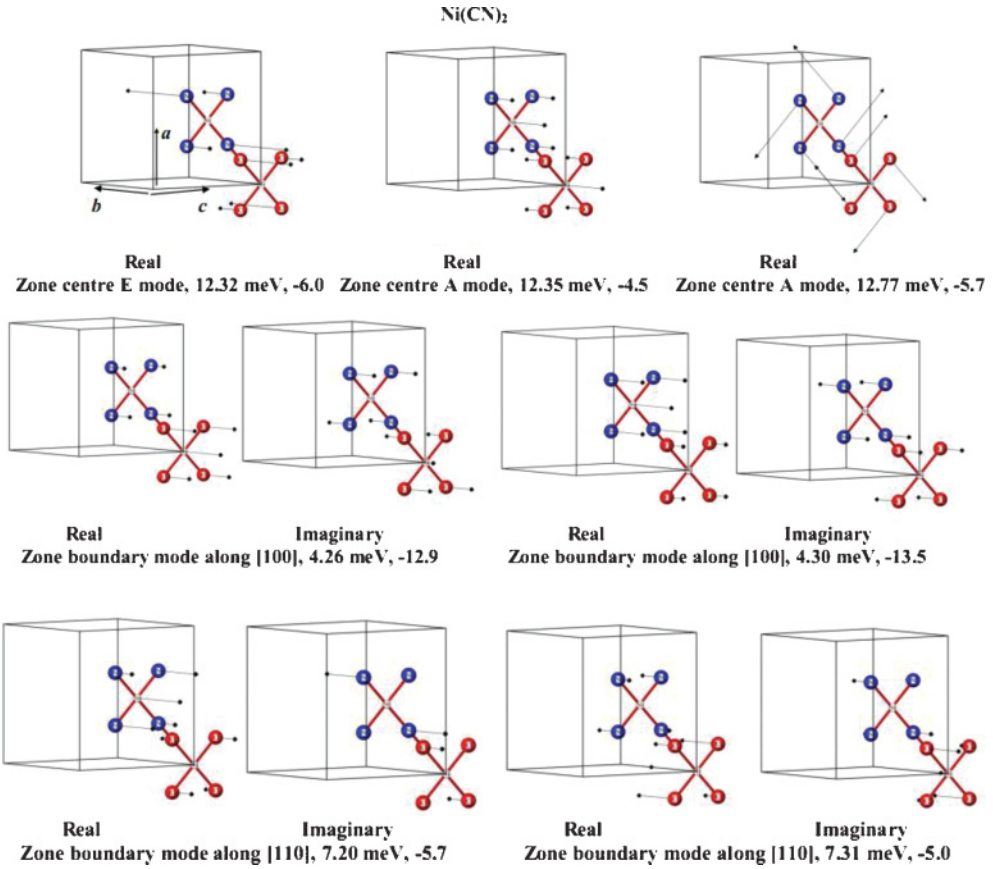

FIG. 17. (Color online) Polarization vector of the zone-center and zone-boundary modes in $Ni(CN)_2$. For each mode the energy and Grüneisen parameter is indicated. The lengths of arrows are related to the displacement of the atoms. The absence of an arrow on an atom indicates that the atom is at rest. At the zone center, where the phase factor is zero, the eigenvectors have only real components. The numbers after the mode assignments give the phonon energies and Grüneisen parameters, respectively. Zone-boundary eigenvectors have both the real and imaginary components. The actual displacements of atoms are a combination of both these components. Key: Ni, gray spheres; C, red spheres; N, blue spheres.

of temperature, the hardening of modes above 2 meV must be owing to large positive explicit anharmonicity of these phonons.

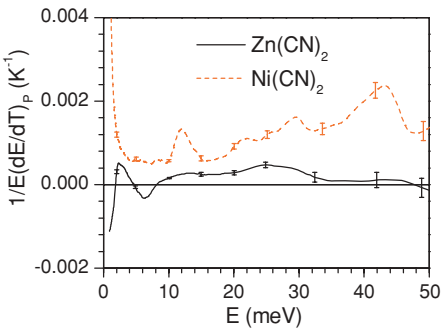

FIG. 18. (Color online) The total anharmonicities ($\frac{1}{E_i}\frac{dE_i}{dT}|_P$) of different phonons of energy E in $Zn(CN)_2$ and $Ni(CN)_2$. The $\frac{1}{E_i}\frac{dE_i}{dT}|_P$ has been obtained using the cumulative distributions of the experimental data of DOS of $Zn(CN)_2$ at 180 and 240 K, while for $Ni(CN)_2$ the experimental data at 160 and 220 K have been used. The inelastic neutron scattering measurements are carried out in the energy-gain mode. The data for $Ni(CN)_2$ at 160 K were obtained only up to 50 meV.

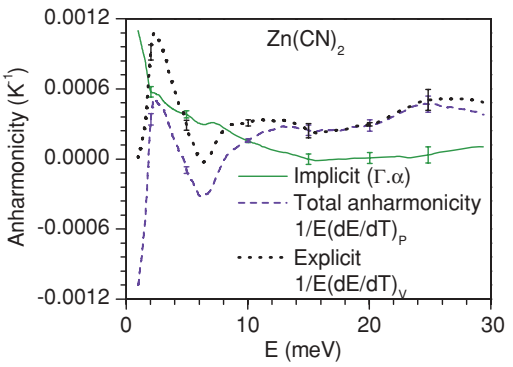

FIG. 19. (Color online) Total anharmonicity, and implicit (quasiharmonic) and explicit (true anharmonic) contributions of different phonons in $Zn(CN)_2$. The total anharmonicity ($\frac{1}{E_i}\frac{dE_i}{dT}|_P$) has been obtained using the cumulative distributions of the experimental data of DOS of $Zn(CN)_2$ at 180 and 240 K. The quasiharmonic contribution has been obtained (Ref. 17) using the pressure dependence of DOS at 165 K. The bulk modulus B value of 34.19 GPa (Ref. 39) has been used for estimating Γ_i values from our measured (Ref. 17) $\frac{\Gamma_i}{B}$ values. The large contributions to the measured spectra from the high-pressure cell did not allow the experimental quasiharmonic contribution for $Zn(CN)_2$ to be obtained beyond 30 meV (Ref. 17). The data have therefore only been shown up to 30 meV.

The present temperature dependence of phonon spectra as well as our previous pressure dependence measurements[17] have been used for obtaining the true anharmonicity of phonons in $Zn(CN)_2$. For materials with negative or positive thermal expansion coefficients (α), the second term on the right-hand side ($\Gamma_i \alpha$) of Eq. (4) is always positive. $Zn(CN)_2$ has negative thermal expansion over its entire temperature range of stability. The quasiharmonic contribution obtained from our previous high-pressure DOS measurements is shown in Fig. 19. The explicit ($\frac{1}{E_i}\frac{dE_i}{dT}|_V$) contribution for phonon modes up to 30 meV in $Zn(CN)_2$ extracted using Eq. (4) is shown in Fig. 19. The magnitude of anharmonicities of modes in these compounds is substantially larger than those in other typical solids,[38] where it ranges between 2×10^{-5} K^{-1} and 10×10^{-5} K^{-1}.

V. CONCLUSIONS

We have reported measurements of the temperature dependence of phonon spectra for $Zn(CN)_2$ and $Ni(CN)_2$ and results of *ab initio* lattice dynamical calculations. The comparison of phonon spectra for Zn and Ni compounds show strong renormalization effects in the phonon spectra of these compounds, which cannot be simply explained by the lattice contraction and mass effect. The phonon spectra have been well reproduced by using *ab initio* calculations. The anomalous thermal expansion bahavior in both the compounds has been estimated. Our calculated NTE coefficient in $Zn(CN)_2$ agrees well with the experimental data. Calculations show that phonon modes of energy $\sim$2 meV are major contributors to NTE. The measured temperature dependence of the phonon spectra along with our previous pressure-dependent phonon measurements has been used for estimating the quasiharmonic and true anharmonicity. The value for the NTE coefficient in the plane of the layered material $Ni(CN)_2$ has been calculated and found to be in excellent agreement with that determined experimentally. We have shown that low-energy phonon modes in these compounds are strongly anharmonic.

ACKNOWLEDGMENT

The University of Reading is thanked for the provision of the Chemical Analysis Facility.

[1] T. A. Mary, J. S. O. Evans, T. Vogt, and A. W. Sleight, Science **272**, 90 (1996).
[2] C. Lind, A. P. Wilkinson, Z. Hu, S. Short, and J. D. Jorgensen, Chem. Mater. **10**, 2335 (1998).
[3] S. J. Hibble, A. M. Chippindale, A. H. Pohl, and A. C. Hannon, Angew. Chem. Int. Ed. **46**, 7116 (2007).
[4] A. L. Goodwin, M. T. Dove, A. M. Chippindale, S. J. Hibble, A. H. Pohl, and A. C. Hannon, Phys. Rev. B **80**, 054101 (2009).
[5] A. L. Goodwin and C. J. Kepert, Phys. Rev. B **71**, R140301 (2005).
[6] A. L. Goodwin, M. Calleja, M. J. Conterio, M. T. Dove, J. S. O. Evans, D. A. Keen, L. Peters, and M. G. Tucker, Science **319**, 794 (2008).
[7] K. W. Chapman, P. J. Chupas, and C. J. Kepert, J. Am. Chem. Soc. **127**, 15630 (2005).
[8] P. Ding, E. J. Liang, Y. Jia, and Z. Y. Du, J. Phys. Condens. Matter **20,** 275224 (2008).
[9] D. J. Williams, D. E. Partin, F. J. Lincoln, J. Kouvetakis, and M. O'Keefe, J. Solid State Chem. **134**, 164 (1997).
[10] W. I. David, J. S. O. Evans, and A. W. Sleight, Europhys. Lett. **46**, 661 (1999).
[11] G. Ernst, C. Broholm, G. R. Kowach, and A. P. Ramirez, Nature (London) **396**, 147 (1998).
[12] Y. Yamamura, N. Nakajima, T. Tsuji, M. Koyano, Y. Iwasa, S. Katayama, K. Saito, and M. Sorai, Phys. Rev. B **66**, 014301 (2002).
[13] R. Mittal, S. L. Chaplot, H. Schober and T. A. Mary, Phys. Rev. Lett. **86**, 4692 (2001).
[14] R. Mittal, S. L. Chaplot, A. I. Kolesnikov, C.-K. Loong, and T. A. Mary, Phys. Rev. B **68**, 054302 (2003).
[15] R. Mittal and S. L. Chaplot, Phys. Rev. B **60**, 7234 (1999).
[16] K. W. Chapman, M. Hagen, C. J. Kepert, and P. Manuel, Physica B **60**, 385 (2006).
[17] R. Mittal, S. L. Chaplot and H. Schober, Appl. Phys. Lett. **95**, 201901 (2009).
[18] D. L. Price and K. Skold, in *Neutron Scattering*, edited by K. Skold and D. L. Price (Academic, Orlando, FL, 1986), Vol. A; J. M. Carpenter and D. L. Price, Phys. Rev. Lett. **54**, 441 (1985).
[19] www.ncnr.nist.gov; V. F. Sears, Neutron News **3**, 29 (1992); *Neutron Data Booklet*, edited by A.-J. Dianoux and G. Lander (Institut Laue-Langevin, Grenoble, France, 2002).
[20] P. E. Blöchl, Phys. Rev. B **50**, 17953 (1994).
[21] P. Hohenberg and W. Kohn, Phys. Rev. **136**, 864 (1964).
[22] W. Kohn and L. J. Sham, Phys. Rev. **140**, 1133 (1965).
[23] G. Kresse and J. Furthmüller, Comput. Mater. Sci. **6**, 15 (1996).
[24] G. Kresse and D. Joubert, Phys. Rev. B **59**, 1758 (1999).
[25] J. P. Perdew, K. Burke, and M. Ernzerhof, Phys. Rev. Lett. **77**, 3865 (1996).
[26] J. P. Perdew, K. Burke, and M. Ernzerhof, Phys. Rev. Lett. **78**, 1396 (1997).
[27] K. Parlinski, Z.-Q. Li, and Y. Kawazoe, Phys. Rev. Lett. **78**, 4063 (1997).
[28] K. Parlinksi, Software phonon 2003.
[29] R. Mittal, S. Mitra, H. Schober, S. L. Chaplot, and R. Mukhopadhyay, e-print arXiv:0904.0963.
[30] T. R. Ravindran, A. K. Arora, Sharat Chandra, M. C. Valsakumar and N. V. Chandra Shekar, Phys. Rev. B **76**, 054302 (2007).
[31] G. Venkataraman, L. Feldkamp, and V. C. Sahni, *Dynamics of Perfect Crystals* (MIT Press, Cambridge, 1975).
[32] F. Birch, J. Geophys. Res. **57**, 227 (1952).
[33] J. W. Zwanziger, Phys. Rev. B **76**, 052102 (2007).
[34] R. Mittal and S. L. Chaplot, Phys. Rev. B **78**, 174303 (2008).

[35]R. Mittal, S. L. Chaplot, S. K. Mishra, and P. P. Bose, Phys. Rev. B **75**, 174303 (2007).

[36]T. Chatterji, P. G. Freeman, M. Jimenez-Ruiz, R. Mittal and S. L. Chaplot, Phys. Rev. B **79**, 184302 (2009); U. D. Wdowik, K. Parlinski, Tapan Chatterji, S. Rols, and H. Schober, *ibid.* **82**, 104301 (2010).

[37]B. A. Weinstein and R. Zallen, in *Light Scattering in Solids IV,* edited by M. Cardona and G. Guntherodt (Springer, Berlin, 1984), p. 463.

[38]R. Zallen and E. M. Conwell, Solid State Commun. **31**, 557 (1979).

[39]K. W. Chapman and P. J. Chupas, J. Am. Chem. Soc. **129**, 10090 (2007).